Magnetic Proximity Effect in YBa$_2$Cu$_3$O$_7$/La$_{2/3}$Ca$_{1/3}$MnO$_3$ and YBa$_2$Cu$_3$O$_7$/LaMnO$_{3+\delta}$ Superlattices

D. K. Satapathy,[1] M. A. Uribe-Laverde,[1] I. Marozau,[1] V. K. Malik,[1] S. Das,[1] Th. Wagner,[1] C. Marcelot,[2] J. Stahn,[2] S. Brück,[3] A. Rühm,[4] S. Macke,[4] T. Tietze,[4] E. Goering,[4] A. Frañó,[5,6] J.-H. Kim,[5] M. Wu,[5] E. Benckiser,[5] B. Keimer,[5] A. Devishvili,[7] B. P. Toperverg,[7] M. Merz,[8] P. Nagel,[8] S. Schuppler,[8] and C. Bernhard[1,*]

[1]University of Fribourg, Department of Physics and Fribourg Centre for Nanomaterials, Chemin du Musée 3, CH-1700 Fribourg, Switzerland

[2]Laboratory for Neutron Scattering Paul Scherrer Institut, CH-5232 Villigen, Switzerland

[3]University of Würzburg, Physikalisches Institut, Am Hubland, D-97074 Würzburg, Germany

[4]Max-Planck-Institut für Intelligente Systeme, Heisenbergstrasse 3, D-70569 Stuttgart, Germany

[5]Max-Planck-Institut für Festkörperforschung, Heisenbergstrasse 1, D-70569 Stuttgart, Germany

[6]Helmholtz-Zentrum Berlin für Materialien und Energie, Wilhelm-Conrad-Röntgen-Campus BESSY II, Albert-Einstein-Str. 15, D-12489 Berlin, Germany

[7]Institute of Solid State Physics, Ruhr-Universität Bochum, D-44801 Bochum, Germany

[8]Karlsruhe Institute of Technology, Institut für Festkörperphysik, D-76021 Karlsruhe, Germany

Using neutron reflectometry and resonant x-ray techniques we studied the magnetic proximity effect (MPE) in superlattices composed of superconducting YBa$_2$Cu$_3$O$_7$ and ferromagnetic-metallic La$_{0.67}$Ca$_{0.33}$MnO$_3$ or ferromagnetic-insulating LaMnO$_{3+\delta}$. We find that the MPE strongly depends on the electronic state of the manganite layers, being pronounced for the ferromagnetic-metallic La$_{0.67}$Ca$_{0.33}$MnO$_3$ and almost absent for ferromagnetic-insulating LaMnO$_{3+\delta}$. We also detail the change of the magnetic depth profile due to the MPE and provide evidence for its intrinsic nature.

The coupling between the antagonistic superconducting (SC) and ferromagnetic (FM) orders in thin film multilayers is the subject of intensive research. The understanding of the SC-FM multilayers comprising conventional elemental or alloy materials is already fairly advanced [1,2]. In comparison, little is known about their oxide counterparts which combine the cuprate high T_c superconductors and the manganites that are well known for their colossal magnetoresistance effect [3,4]. A few groups have been growing YBa$_2$Cu$_3$O$_7$/La$_{2/3}$Ca$_{1/3}$MnO$_3$ (YBCO/LCMO) multilayers [5–10] and observed a range of interesting effects, like a giant magnetoresistance [11], a large photo-induced T_c increase [12], a magnetic proximity effect (MPE) [13–16] where a FM Cu moment is induced in the YBCO layers, a reconstruction of the orbital occupation and symmetry of the interfacial CuO$_2$ layers [17], and even a SC-induced modification of the FM order [16]. These effects are thought to be closely related to the strong electronic correlations and the intimate coupling between the magnetic, orbital and lattice degrees of freedom in these oxides. These yield a manifold of nearly degenerate ground states with a rich spectrum of properties that can be readily tuned with external parameters. The cuprate high T_c superconductors are indeed close to a magnetic instability where a spin-density-wave is induced with impurities [18,19] or magnetic fields [20]. The manganites have also extremely versatile electromagnetic properties that are strongly modified by strain pressure or a magnetic field [4]. It is thus not unexpected that the proximity effect in these oxide SC-FM superlattices (SLs) is more complex than in their classical counterparts and involves an unusual magnetic component that remains to be understood.

Here we establish that the electronic and/or orbital properties of the manganite layers are playing a decisive role in the MPE. We show that the MPE is almost absent in SLs with ferromagnetic, insulating (FM-I) LaMnO$_{3+\delta}$ (LMO) layers and we detail how the MPE affects the FM depth profile for a SL with ferromagnetic, metallic (FM-M) LCMO layers.

Superlattices of [YBCO(10 nm)/LCMO(10 nm)]$_{10}$ and [YBCO(10 nm)/LMO(10 nm)]$_{10}$ were grown with pulsed laser deposition on La$_{0.3}$Sr$_{0.7}$Al$_{0.65}$Ta$_{0.35}$O$_3$ (LSAT) (001) substrates ($10 \times 10 \times 0.5$ mm^3) and characterized as described in Ref. [21]. The SC onset temperatures are $T_c^{\mathrm{ons}} \approx$ 88 and 77 K and the FM ones are $T^{\mathrm{Curie}} \approx$ 200 and 140 K, respectively. As outlined in Ref. [22], the LMO layers are nonstoichiometric and thus hole doped to a FM-I state [23].

Polarized neutron reflectometry (PNR) measurements were performed with the two-axis diffractometers AMOR at SINQ of PSI in Villigen, CH, NREX of FRM-II in Munich, D, and SUPERADAM of ILL in Grenoble, F. Magnetic fields up to 4 kOe oriented perpendicular to the scattering plane and parallel to the film surface were produced with Helmholtz coils. The samples were cooled with closed-cycle cryostats in an applied magnetic field. Data
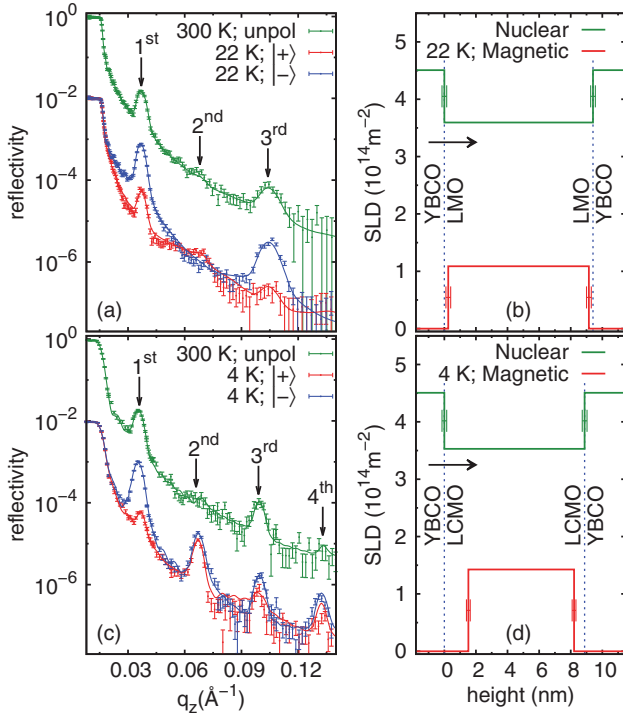
FIG. 1 (color). PNR curves for spin-up ($|+\rangle$) and spin-down ($|-\rangle$) polarization of (a) $[\text{YBCO}(10 \text{ nm})/\text{LMO}(10 \text{ nm})]_{10}$ and (c) $[\text{YBCO}(10 \text{ nm})/\text{LCMO}(10 \text{ nm})]_{10}$. Also shown are unpolarized curves at 300 K. Arrows mark the position of the SLBPs. The curves are vertically shifted for clarity. (b) and (d): Depth profiles as obtained from fitting the data in (a) and (c) (solid lines) of the nuclear (green line) and magnetic (red line) scattering length densities (SLD) which are proportional to the nuclear and magnetic potentials, respectively. Arrows point along the SL growth direction. The error for the SLD in (b) and (d) is smaller than the line thickness; all the error bars in these two figures were obtained as described in Ref. [22].

fitting was performed with the program SUPERFIT [24]. The x-ray magnetic circular dichroism (XMCD) was measured at the beam lines UE56/2-PGM1 at BESSY II, Helmholtz Center Berlin, D, and WERA at ANKA in Karlsruhe, D. The x-ray resonant magnetic reflectometry (XRMR) was measured on UE56/2-PGM1 using the MPI-IS ErNST endstation. Data simulation was performed with the program REMAGX [25]. Details about the XRMR technique are given in Refs. [22,26].

Figure 1 displays our specular PNR data on the YBCO/LMO and YBCO/LCMO SLs that establish that the MPE strongly depends on the electronic properties of the FM layers. Figures 1(a) and 1(c) compare the PNR curves at $T \ll T^{\text{Curie}}$. They confirm that the LMO and the LCMO layers are both strongly FM. This is evident from the large splitting of the spin-up and spin-down polarized curves around the 1st order superlattice Bragg peak (SLBP) which is a measure of the average magnetization density of the SL. The best fits (solid lines) with a simple model of blocklike potentials yield an average moment per Mn ion

of $2.3 \mu_B$ for both LMO and LCMO, which agrees well with the saturation value of 2.4 and $2.3 \mu_B$ from dc magnetization (see Ref. [22]). Despite these comparable FM moments, these SLs have remarkably different magnetic depth profiles. This is evident from the marked difference of the PNR curves in the vicinity of the 2nd and 4th order SLBPs. The even order SLBPs should have a very small intensity since they are symmetry forbidden due to the similar thicknesses of about 10 nm of the YBCO and LMO or LCMO layers. The intensities of the 2nd and 4th SLBP are indeed strongly suppressed for the curves at 300 K where only the nuclear potentials contribute.

For the SL with the FM-I LMO layers in Fig. 1(a) the intensity of the 2nd and 4th order SLBPs remains weak even at $T \ll T^{\text{Curie}}$. This confirms that the magnetic potential essentially maintains the symmetry of the nuclear one, i.e., that the magnetization is not strongly modified by a MPE. The magnetic depth profile in Fig. 1(b) obtained from fitting the data in Fig. 1(a) (solid lines) shows indeed that the FM order persists throughout the LMO layers and disappears close to the LMO/YBCO interfaces, i.e., within the combined error bar of the nuclear and magnetic potential widths of about 1.5 Å. In clear contrast, for the FM-M LCMO, a pronounced 2nd order SLBP develops below T^{Curie}. This highlights that the profile of the magnetic potential is substantially different from the nuclear one. This effect was previously noted [13–15] and interpreted in terms of two possible magnetic depth profiles. The so-called inverse proximity effect model assumes an induced Cu moment in the YBCO layers that is antiparallel to the Mn one. Alternatively, the dead layer or better depleted layer model (as we argue below) involves a suppression of the FM order of the Mn moment on the LCMO side of the interface [27,28]. The previous PNR data contained only the 1st and 2nd order SLBPs which made it difficult to distinguish between these two possibilities. The accessible range of scattering vectors was limited by the quality of the SLs and, in particular, by the buckling of the SrTiO_3 substrates which develops below 100 K in the context of a structural transition [16,29]. This problem has been avoided for our new SLs on LSAT substrates [21]. Our PNR curves extend with a sufficient signal to noise ratio to the 4th order SLBPs and thus provide the additional information that is required for an unambiguous identification of the magnetic depth profile. In particular, as shown in Fig. 1(d), they confirm the depleted layer model where the FM order of the Mn moments is strongly reduced on the LCMO side of the interface. In these fits we neglected the induced FM Cu moments in the YBCO layers that are addressed below. They are much smaller than the Mn moments which thus govern the main features of the PNR curves. Interestingly, the depleted FM layers are significantly thinner at the top interface than at the bottom one, as seen from the film surface. Whether this effect is caused by a difference of the atomic layer sequence or the
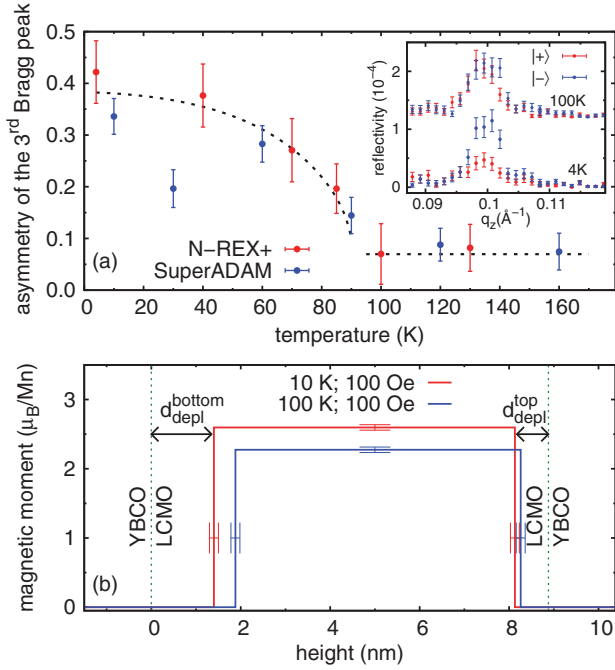
FIG. 2 (color). (a) T dependence of the asymmetry between the peak intensities of the spin-down and spin-up polarized curves at the 3rd order SLBP showing an anomalous order-parameter-like increase below T_c. Inset: Magnification around this peak above and well below T_c. (b) Corresponding changes of the magnetic depth profile.

FIG. 3 (color online). XMCD spectra in TEY mode at the L edges of Mn and Cu plotted in terms of the dichroism, $I^+ - I^-$, for (a) YBCO/LCMO and (b) YBCO/LMO. Inset: Corresponding normalized x-ray absorption spectra.

interface roughness remains to be further investigated. Notably, the magnetic potentials at 10 and 100 K, as shown in Fig. 2(b), exhibit some characteristic differences; i.e., the value of $d_{\mathrm{depl}}^{\mathrm{bottom}}$ is reduced by about 5 Å, whereas $d_{\mathrm{depl}}^{\mathrm{top}}$ is hardly changed. A more detailed T-dependent study has been performed for the vicinity of the 3rd order SLBP where the changes between the curves at 10 and 100 K are most pronounced. Figure 2(a) shows that the spin polarization dependent splitting of the intensity of this SLBP exhibits an anomalous change in the vicinity of the SC transition of YBCO. It remains very small above 90 K and exhibits an order-parameter-like increase below $T_c^{\mathrm{ons}} \approx 88$ K. A corresponding set of complete PNR curves would be required to establish whether this SC-induced anomaly involves a changes of the depleted layer thickness or rather a modification of the magnetic roughness, for example, due to changes in the FM domain structure. Irrespective of this open question, the mere observation of this SC-induced anomaly implies that the coupling between the SC order in the YBCO layers and the magnetic one in LCMO is maintained despite the depleted layer. The later thus should not be mistaken for a magnetically dead layer but may host an antiferromagnetic or oscillatory component which cannot be detected with the specular PNR. The comparison between the LMO and LCMO SLs certainly points toward an intrinsic MPE that is intimately
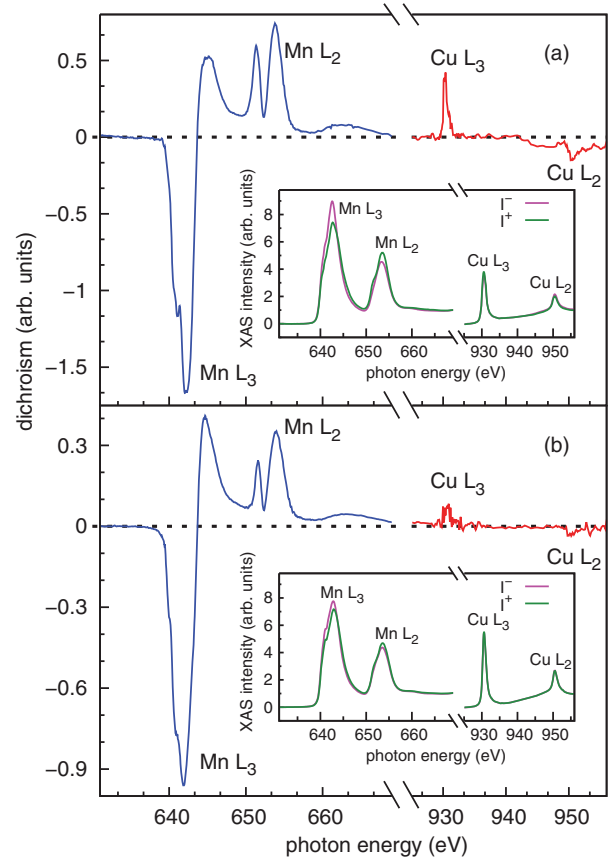
related to the electronic (orbital) properties of the FM manganite layers (more evidence is presented in Ref. [22]).

Further insight into the MPE has been obtained with XMCD measurements which provide element specific magnetic information. As was previously noted [15], they reveal a FM moment of the Cu ions. Our new observation is that this Cu moment is significantly larger for FM-M LCMO than for the FM-I LMO. Figure 3 shows the XMCD difference spectra around the L_3 and L_2 edges of Mn and Cu as obtained in total electron yield (TEY) mode. For YBCO/LCMO in Fig. 3(a) they reveal a sizeable average Cu moment per electron hole in the Cu $3d$ shell with an spin component of $0.23 \pm 0.1 \mu_B/n_h$ (the orbital one is much smaller). For YBCO/LMO in Fig. 3(b) it amounts only to about $0.03 \pm 0.01 \mu_B/n_h$. The orientation of the Cu moment with respect to the Mn one is, in both cases, antiparallel as is evident from the opposite sign of the XMCD signals at the L_3 and L_2 edges of Cu and Mn. This Cu moment was previously explained as a consequence of antiferromagnetic superexchange interactions across the interface [15]. Our new PNR and XMCD data establish that these induced Cu moments exist despite the depleted FM layer on the LCMO side of the interface.
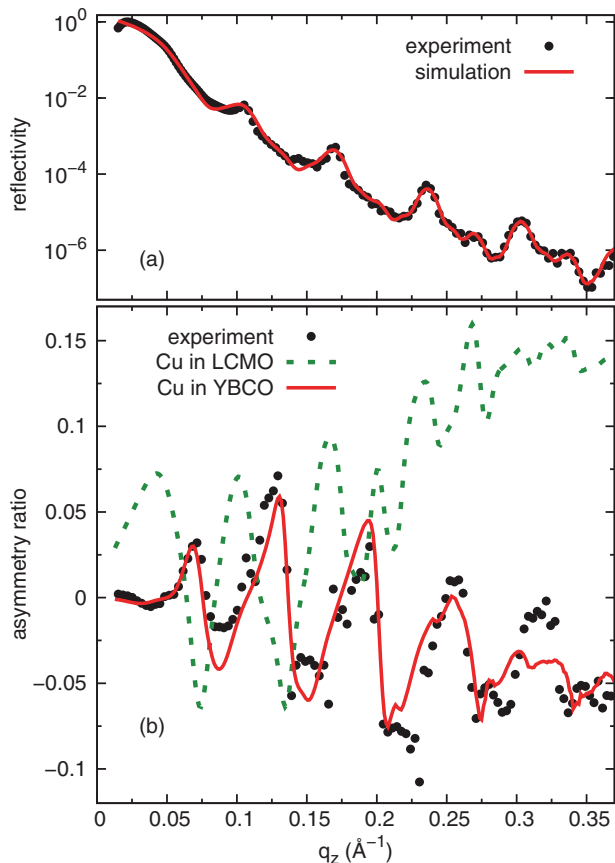
FIG. 4 (color). (a) Resonant x-ray reflectometry curve at the Cu L_3 edge of YBCO/LCMO obtained at 300 K. (b) Difference curve between positive and negative x-ray helicity at 40 K containing the information about the depth profile of the FM Cu moments. The simulations have been performed for the cases where the Cu moments reside in the YBCO layers (red line) and the LCMO layers (green dashed line), respectively.

within the FM manganite layers, for example, due to chemical interdiffusion or another kind of cross contamination during pulsed laser deposition growth. The XMCD technique in the TEY mode is indeed very surface sensitive and does not probe the spatial distribution of the magnetic moments. Therefore, we have also performed XRMR measurements near the Cu L_3 edge which allow one to probe how the Cu ions and their respective magnetic moments are distributed throughout the entire SL. The unpolarized reflectivity curve at 300 K in Fig. 4(a) contains information about the depth profile of the concentration of the Cu ions. The red line shows the result of a simulation with a simple blocklike depth profile of the complex chemical potentials (see Ref. [22]) which reproduces the period and the intensity of the main peaks and confirms the ~20 nm thickness of the YBCO/LCMO bilayers. The information about the corresponding magnetic depth profile of the Cu moments is contained in the asymmetry (difference) curve between positive and negative x-ray helicity at 40 K, as shown in Fig. 4(b). This asymmetry curve contains a series of pronounced and equally spaced peaks which highlight that the FM Cu moments are periodically distributed throughout the SL. The red line shows the result of a simulation where the FM Cu moments are placed within the YBCO layers (for simplicity we also used blocklike magnetic profiles). Based on the XMCD data we assume that the Cu moments are antiparallel to the Mn moments whose direction is determined by the external magnetic field and we use a Cu moment of about $0.25 \pm 0.1 \mu_B$. While the fit could be further improved, for example, by grading the profile of the Cu moments in the YBCO layers, it already reproduces quite well the main features of the data, such as the peak positions and their intensity variation. Most importantly, the simulation for the opposite case where the Cu moments are assumed to reside within the LCMO layers (dashed green line) is in disagreement with the data. The Cu moments are now placed on the opposite side of the interface which gives rise to a π phase shift of the reflected x-ray waves and thus to an exchange of the maxima and minima of the asymmetry curve. A reasonable agreement with the data could only be obtained by changing the mutual orientation of the Cu and Mn moments from antiparallel to parallel. This possibility is however excluded by the XMCD data in Fig. 3 which highlight that the Cu and Mn moments are antiparallel. Our combined XMCD and XRMR data thus provide compelling evidence that the FM Cu ions originate from the YBCO layers.

In summary, we performed polarized neutron reflectometry, x-ray circular dichroism, and x-ray resonant magnetic reflectometry measurements on YBCO/LCMO and YBCO/LMO SLs whose FM manganite layers are metallic and insulating, respectively. We found that the MPE is governed by the electronic (orbital) state of the FM manganite layers. Furthermore, we detailed the MPE induced changes of the magnetic depth profile and provided direct

Notably, the induced Cu moment is even significantly smaller for the YBCO/LMO SL where a large FM Mn moment persists to the interface. Once more this suggests that the depleted layers host a strong magnetic order that cannot be detected with PNR and XMCD (which are only sensitive to FM components). The induced Cu moment on the YBCO side and the strong modification of the FM order of the Mn moments on the LCMO side of the interface are likely caused by the same mechanism; a possible scenario in terms of a covalent bonding across the interface that involves the $3d_{z^2-r^2}$ orbitals of Cu and Mn is outlined in Ref. [17]. The strong suppression of this MPE for the FM-I LMO may well be related to the formation of orbital polaron arrays and other orbitally ordered states [30] that start to compete with the interfacial covalent bonding as the manganite layers become less hole doped and insulating.

Finally, we address the concern that the signal of the FM moments in the Cu-XMCD data may arise from a small number of Cu ions that are unintentionally incorporated

4

evidence that the induced Cu moments reside within the YBCO layers. Our results thus provide evidence for an intrinsic nature of the MPE and an intimate magnetic coupling across the cuprate-manganite interfaces.

*christian.bernhard@unifr.ch

[1] A. Buzdin, Nature Mater. **3**, 751 (2004).
[2] M. Eschrig, Phys. Today **64**, 43 (2011).
[3] R. von Helmolt, J. Wecker, B. Holzapfel, L. Schultz, and K. Samwer, Phys. Rev. Lett. **71**, 2331 (1993).
[4] Y. Tokura and Y. Tomioka, J. Magn. Magn. Mater. **200**, 1 (1999).
[5] P. Przyslupski, S. Kolesnik, E. Dynowska, T. Skoskiewicz, and M. Sawicki, IEEE Trans. Appl. Supercond. **7**, 2192 (1997).
[6] A. Goldman, P. Kraus, K. Nikolaev, V. Vas'ko, A. Bhattacharya, and W. Cooley, J. Supercond. **14**, 283 (2001).
[7] H.-U. Habermeier, G. Cristiani, R. Kremer, O. Lebedev, and G. van Tendeloo, Physica C (Amsterdam) **364–365**, 298 (2001).
[8] Z. Sefrioui, D. Arias, V. Peña, J. E. Villegas, M. Varela, P. Prieto, C. León, J. L. Martinez, and J. Santamaria, Phys. Rev. B **67**, 214511 (2003).
[9] T. Holden, H.-U. Habermeier, G. Cristiani, A. Golnik, A. Boris, A. Pimenov, J. Humlíček, O. I. Lebedev, G. Van Tendeloo, B. Keimer, and C. Bernhard, Phys. Rev. B **69**, 064505 (2004).
[10] R. Werner, C. Raisch, A. Ruosi, B. A. Davidson, P. Nagel, M. Merz, S. Schuppler, M. Glaser, J. Fujii, T. Chassé, R. Kleiner, and D. Koelle, Phys. Rev. B **82**, 224509 (2010).
[11] V. Peña, Z. Sefrioui, D. Arias, C. Leon, J. Santamaria, J. L. Martinez, S. G. E. te Velthuis, and A. Hoffmann, Phys. Rev. Lett. **94**, 057002 (2005).
[12] V. Peña, T. Gredig, J. Santamaria, and I. .K. Schuller, Phys. Rev. Lett. **97**, 177005 (2006).
[13] J. Stahn et al., Phys. Rev. B **71**, 140509 (2005).
[14] A. Hoffmann, S. G. E. te Velthuis, Z. Sefrioui, J. Santamaría, M. R. Fitzsimmons, S. Park, and M. Varela, Phys. Rev. B **72**, 140407 (2005).
[15] J. Chakhalian et al., Nature Phys. **2**, 244 (2006).
[16] J. Hoppler et al., Nature Mater. **8**, 315 (2009).
[17] J. Chakhalian, J. W. Freeland, H.-U. Habermeier, G. Cristiani, G. Khaliullin, M. van Veenendaal, and B. Keimer, Science **318**, 1114 (2007).
[18] H. Alloul, J. Bobroff, M. Gabay, and P. J. Hirschfeld, Rev. Mod. Phys. **81**, 45 (2009).
[19] A. Suchaneck, V. Hinkov, D. Haug, L. Schulz, C. Bernhard, A. Ivanov, K. Hradil, C. T. Lin, P. Bourges, B. Keimer, and Y. Sidis, Phys. Rev. Lett. **105**, 037207 (2010).
[20] B. Lake et al., Nature (London) **415**, 299 (2002).
[21] V. K. Malik et al., Phys. Rev. B **85**, 054514 (2012).
[22] See Supplemental Material at http://link.aps.org/supplemental/10.1103/PhysRevLett.108.197201 for magnetic and transport properties of YBCO/LCMO and YBCO/LMO superlattices, including additional experimental details for resonant x-ray absorption and reflectometry techniques.
[23] Z. Marton, S. S. A. Seo, T. Egami, and H. N. Lee, J. Cryst. Growth **312**, 2923 (2010).
[24] SUPERFIT: Polarized Neutron Reflectivity Tool (Max-Planck Institute for Intelligent Systems, Stuttgart).
[25] S. Macke, S. Brück, and E. Goering, REMAGX: X-Ray Magnetic Reflectivity Tool, Max-Planck Institute for Intelligent Systems, Stuttgart, (2010).
[26] S. Brück, S. Bauknecht, B. Ludescher, E. Goering, and G. Schütz, Rev. Sci. Instrum. **79**, 083109 (2008).
[27] W. Luo, S. J. Pennycook, and S. T. Pantelides, Phys. Rev. Lett. **101**, 247204 (2008).
[28] P. Przyslupski, I. Komissarov, W. Paszkowicz, P. Dluzewski, R. Minikayev, and M. Sawicki, Phys. Rev. B **69**, 134428 (2004).
[29] J. Hoppler, J. Stahn, H. Bouyanfif, V. K. Malik, B. D. Patterson, P. R. Willmott, G. Cristiani, H.-U. Habermeier, and C. Bernhard, Phys. Rev. B **78**, 134111 (2008).
[30] J. Geck, P. Wochner, S. Kiele, R. Klingeler, A. Revcolevschi, M. v Zimmermann, B. Büchner, and P. Reutler, New J. Phys. **6**, 152 (2004).